Digest Journal of Nanomaterials and Biostructures Vol. 12, No. 2, April - June 2017, p. 533 - 547

MORPHOLOGICAL AND OPTICAL CHARACTERIZATION OF Mg-ZnO THIN FILMS DEPOSITED BY CO-MAGNETRON SPUTTERING TECHNIQUE

S. E. ALOMAIRY[a*], H. M. ALI[b] , M. M. ABD EL-RAHEEM[a,b],
A. M. AL-BARADI[a], F. ABDEL-WAHAB[a,c], S. A. AMIN[d]
[a]Department of physics, Faculty of Science, Taif University, Taif 888, KSA
[b]Department of physics, Faculty of Science, Sohag University, Sohag 82524, Egypt
[c]Department of physics, Faculty of Science, Aswan University, Aswan. Egypt
[d]Department of physics, Faculty of Science, Assiut University, Assiut 71516. Egypt

This paper reports the structural and optoelectronic properties of prepared pure and Mg doped ZnO nanoparticles using co-magnetron sputtering technique. The phase purity and crystallites size of synthesized ZnO and Mg doped nanoparticles were characterized and examined using X-ray diffractometar XRD and scanning electron microscopy SEM . The elemental analysis was examined by using energy-dispersive X-ray spectroscopy EDX. The optical properties E_{op} were carried out by using U-V-VIS double beam spectroscopy to study the optoelectronic properties of the thin films under test. The power on Mg target (ratio of Mg) affected the structural parameters such as lattice constant, grain size, strain e as well as the optical parameters such as Urbach tail, optical energy gap, refractive index and carrier concentration.

(Received March 18, 2017; June 1, 2017)

Keywords: sputtering; thin film; Mg-ZnO; optical gap; refractive index.

1. Introduction

A great deal of attentions have been paid to the transparent conductive oxide (TCO) thin films due to their plenty applications such as transparent electrodes in flat panel displays, touch panels and solar cells. Zinc oxide (ZnO) is one of the most promising TCO materials because ZnO is an abundant, low-cost, and non-toxic material [1]. The intrinsic n-type semi-conductivity of ZnO arises from such structural defects as oxygen vacancies and zinc interstitials [2]. For improving its electrical conductivity, ZnO was doped with other metal elements such as boron, aluminum, gallium, magnesium etc. The resistivity of MZO thin films are over 10^5 Ω cm and nearly equivalent to the resistivity of intrinsic ZnO. To promote the electrical conductivity of MZO films, it was suggested that extra dopant be added to the MZO thin films such as gallium [3]. There are few limitations in the application of pure ZnO for integrated optical devices which require a much wider band gap [4]. The band gap of ZnO can be tailored by alloying ZnO with group II elements e.g. Be, Mg, Ca, Cd, and Sr [5]. Moreover, the radius of the Mg^{2+} ion (0.57 Å) closely matches with the radius of Zn^{2+} ion (0.60 Å), so the incorporation of Mg^{2+} ion into ZnO lattice is quite favorable, thus forming MZO. The MZO thin films can be synthesized using various techniques such as RF sputtering, molecular-beam epitaxy, sol–gel, pulse laser deposition and chemical vapor deposition [6]. So the study of the effect of thermal treatment on the structural and optical properties of the optical properties of ZnO can be controlled by changing the energy band gap of ZnO through doping it with wide band gap materials. It has been indicated that the energy band gap of ZnO could be changed from 3.24 eV to 4.0 eV by doping zinc oxide with magnesium oxide (MgO) of wide band gap 7.70 eV [7]. Modification of the band gap and save the lattice constants similar to each other are essential to construct a hetereojunction of two different materials [8].

---

[*] Corresponding author: s.alomairy@tu.edu.sa

The band gap of alloy $Mg_xZn_{1-x}O$ films are in the range from 3.3 to 4.00 eV because magnesium oxide (MgO) has wider band gap energy (7.9 eV) compared with ZnO (3.3 eV). Meanwhile, MgxZn1−xO have ZnO wurtzite structure in case the content of Mg in the films is up to 0.49 [9- 10]. Thence, alloy $Mg_xZn_{1-x}O$ has been considered as an appropriate ternary alloy system that can construct efficient heterojunction with ZnO [11]. It was found that as Mg concentration x increases, the values of the refractive index n decreases and the index dispersions become smaller [12]. It was revealed that, with the rise of annealing temperature the crystallinity and the surface roughness of the MZO films were increased whereas the optical transmittance and the energy band gap were decreased [13]. It was observed that the XRD peak related to (002) plane shifted systematically towards higher angle with the increase in annealing temperature i.e., from 34.471 to 34.571 for MZO and from 34.491 to 34.601 for other MZO [13]. The reason of this peak shifting was the change of stress, firstly due to the increase in annealing temperature [14- 15] additionally due to the increase in Mg concentration [16]. The XRD analysis revealed that, the FWHM of the peak corresponds to (002) plane was narrowed with increasing annealing temperature [13], indicating improvement in crystallinity [17]. It was also found that lower boundary of the grain size was gradually enlarged with enhancing annealing temperature for MZO films. This could be due to the coalescences of grains at higher annealing temperatures [17]. By comparing the lower boundary of the grain size of MZO and the other MZO for identical annealing temperature, it could be pronounced that Mg incorporation slightly deteriorates the crystallinity of the thin films [13]. From reflectance and absorption measurements, the obtained band gap energy tends to augment from 3.287 to 3.827 eV as the doping content (Mg) increases [17]. This widening of the optical band gap is explained by the Burstein-Moss effect which causes a significant increase of electron concentration ($2.89x10^{18}$- $5.19x\ 10^{20}cm^{-3}$). These crystallites were found to be randomly distributed and irregularly disoriented. The grain size was found to decrease from 109 nm to 55 nm as the MgO content varied from 0 to 40% suggesting that there is coalescence of small grains for high doped ZnO samples [17]. It was observed that that the average reflectance is found to vary from 75 to 93% in the visible region for all the samples and the reflectance increases about 50 to 70% as the MgO doping content increases. It was observed clearly a blue-shifting of the absorption spectra towards the UV region, indicating an increase of the band gap. Further, the values of E_g increased with increasing Mg doping. Nidhi Adhlakra and et. al. [18] have reported similar results for doped ZnO samples with MgO concentrations between and 50%. However, this increment in the band gap E_g was believed to be caused by the Burstein-Moss effect [19-21]. Shan et al. [19] have demonstrated that the Mg doping in ZnO leads to an obvious increase in the carrier concentration and a blue shift of the band gap. A. Ghosh et al. [21] have showed that the variation in the optical band gap is analyzed in terms of Burstein-Moss band gap widening. It was reported that the optical energy gap of $Zn_xMg_{1-x}O$ increases with increasing the content of Mg [22]. Zhao-Hui Li et. al. [23] shown that the grain size of the ZnO-like hexagonal phase (Zn, Mg)O decreased as the Mg content increased. But the transmittance and optical band gap of (Zn, Mg)O films increased with the increase of the Mg content [23].

As far as the authors know that a little attention has been paid to study the structural and optical properties of Mg-ZnO thin films prepared by co-magnetron sputtering technique whereas MgO-ZnO has been studied extensively. So, in the present work, the structural and optical properties of Mg-ZnO deposited by co-magnetron sputtering technique are studied.

2. Experimental

The Mg-ZnO films were deposited on silicon substrates in a UNIX 350 magnetron sputtering system with a base pressure of 2×10^{-2} mbar. The sintered ceramic targets of ZnO (purity 99.99%) and Mg (purity 99.99%) were employed as the source material. An argon Ar (99.999%) was used as sputtering gas. The separation between the substrate and target was 10 cm. During the film deposition, the argon pressure maintained at $2.5x10^{-3}$ torr. The angle between the target and substrate was 70^o. The dc sputtering power on ZnO target was 100W , the rf power on Mg target was varying between 0 W to 100 W. The substrate temperature was kept at room temperature. The structure of films was measured by a Rigaku D/Max- A Xray diffractometer (Cu

K radiation, = 1.54178A, ° 40KV, 60 mA). The average grain size of the samples was determined by measuring the FWHM values of the strongest peak of the XRD and estimated by using the relation of Scherrer formula [24]. Optical transmission measurements were carried out over the wavelength range of 300–1200 nm using a Jasco UV-VIS double beam spectrophotometer. The absorption coefficient α of the films was determined from the spectrophotometer reading using the following formula [25]:

$$\alpha = \frac{2.303}{d}\log(\frac{1-R}{T}) \qquad (1)$$

d is the thickness of the film, T is the transmittance and R is the reflectance of the film.

The optical energy gap E_{op} was estimated from the optical measurements by analyzing the optical data with the expression for the optical absorbance, and the photon energy, $h\upsilon$ using the equation [26]:

$$(\alpha h\upsilon)^2 = A(h\upsilon - E_{op}) \qquad (2)$$

A is a constant and h is the Planck's constant. The optical energy gap was obtained by extrapolating the linear portions of the plots of $(\alpha h\upsilon)^2$ versus $h\upsilon$ to $\alpha = 0$.

The Urbach tail E_u of the thin films under test was determined from the linear slope of the curve $\mathrm{Ln}\alpha$ vs photon enrgy using the equation [27]:

$$\alpha = \alpha_o \exp(\frac{h\nu}{E_u}) \qquad (3)$$

The refractive index n for weak and medium absorption regions is given as [28]:

$$n = [N + (N^2 - n_s^2)^{\frac{1}{2}}]^{\frac{1}{2}} \qquad (4)$$

$$N = 2n\frac{T_{Max} - T_{Min}}{T_{Max}T_{Min}} + \frac{s^2+1}{2}$$

$$s = \frac{1}{T_s}\sqrt{\frac{1}{T_s}} - 1$$

and

$$N = \frac{2s}{T_{Min}} + \frac{s^2}{2}$$

for transparent region.

s is the refractive index of the quartz substrate, T_{Max} and T_{Min} are the transmission maximum and the corresponding minimum at a certain wavelength λ, s and T_s are the refractive index and the transmittance of the substrate respectively.

The real part ε_1 of the complex dielectric function ε can be written as [29]:

$$\varepsilon_1 = n^2\text{-}\,k^2 = \varepsilon_\infty - \frac{e^2}{\pi C^2}\frac{M}{m^*}\lambda^2 \qquad (5)$$

ε_∞ is the residual dielectric constant, C is the velocity of light, N is the concentration of the free carrier, m* is the electron effective mass ($=0.24m_o$ for ZnO)

3. Results and discussions

3.1 Energy dispersive X-ray analysis

The EDX analysis reveal that the 0 watt on Mg target and 100 watt on ZnO target, there is no Mg content in the grown film as shown in Fig. 1-a. Raising the power on Mg target resulted in increasing the content of Mg 0, 1.66, 0.27, 1.43, 1.53, and 1.79 for power 0, 20 watt, 40 watt, 60 watt, 80 watt and 100 watt respectively, whereas, ratio of oxygen and magnesium were around 39 and 44 respectively as shown in Fig. 1-b, c, d, e,f.

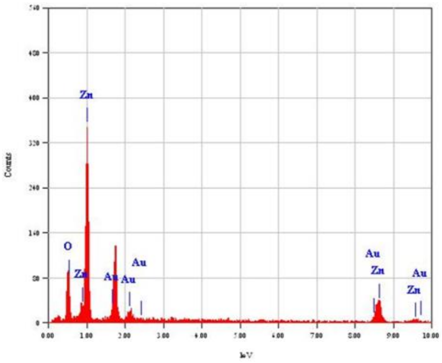

Fig. 1-a: ZnO only

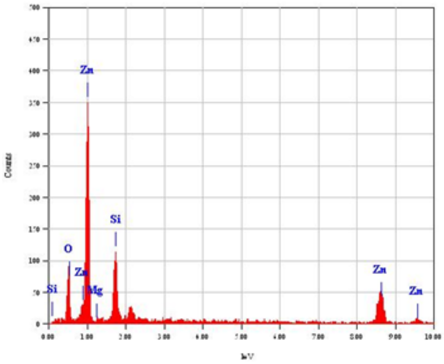

Fig. 1-b: 20 watt on Mg target.

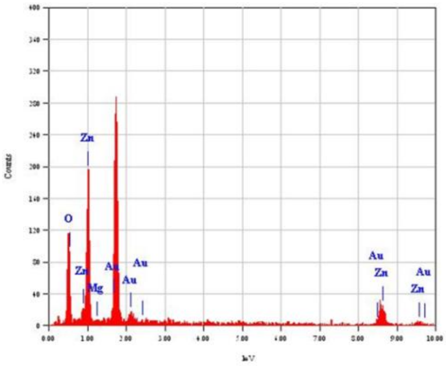

Fig.1-c: 40 watt on Mg target.

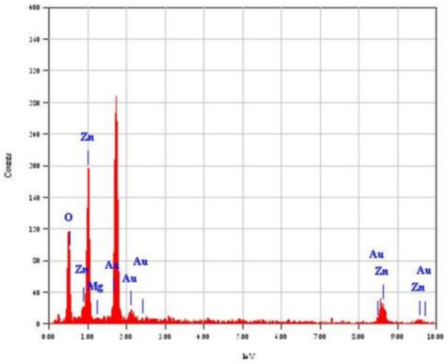

Fig.1-d: 60 watt on Mg target.

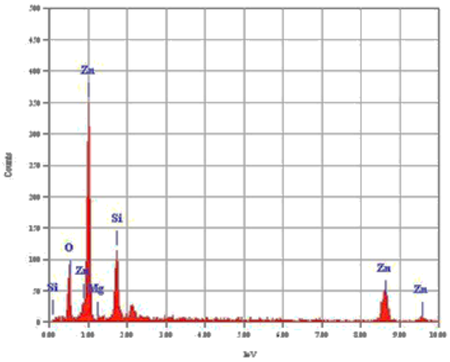

Fig. 1-e: 80 watt on Mg target

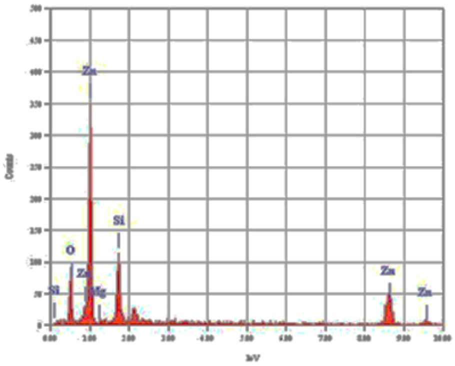

Fig. 1-f: 100 watt on Mg target.

3.2 Scan electron micrograph

The scan electron micrograph indicate that increasing Mg content leads to increasing the grain size as seen in Figs.2-a,b,c.

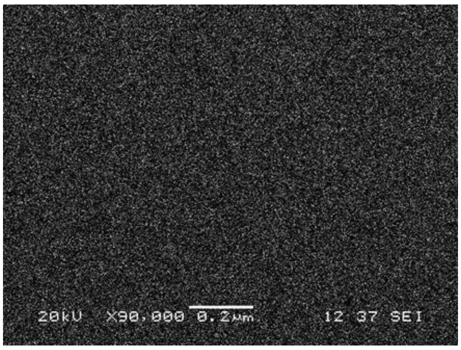

Fig.2-a: Zn O only

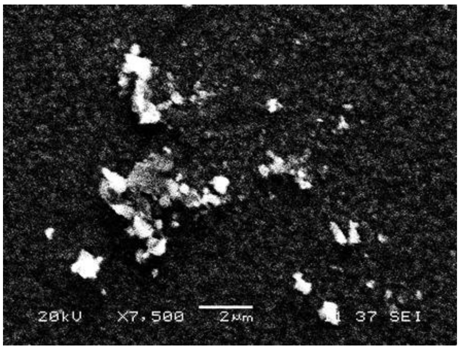

Fig.2-b: 40 watt on Mg target

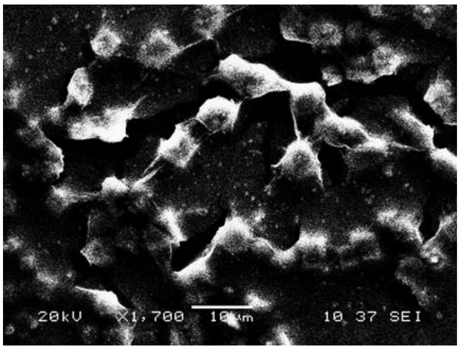

Fig.2-c: 80 watt on Mg target

3.3 X-ray diffraction result

The X-ray micrograph showed that there is a peak related to (002) plane shifted towards lower angle such as 34.58, 34.27, 34.22, 34.19, 34.16 with increasing the power on Mg target 0, 20, 40, 60, 80 watt respectively as seen in Fig.3. The reason of this peak shifting probably is due to the change of stress. Figure 4shows the out of plane c lattice parameter derived from 2θ-s as a function of the power on Mg target. The c lattice parameter increased from 4.995 A^o to 5.031 A^o with increasing the power on Mg target. The crystallite sizes D were calculated using Debye-Scherrer equation [30]:

$$D = \frac{0.9\lambda}{\beta cos\theta}$$

where λ is the wavelength of X-ray used in XRD, β is the full-width at half maximum FWHM and 2θ is the angle at which peaks exist. The grain size values found to increase from 9.13 nm to 17.18

nm with increasing the power on Mg target from 20watt to 80watt. The strain ξ of the films under test was calculated by the equation [31]:

$$\xi = \left[\frac{\lambda}{D\cos\theta} - \beta\right] \text{x} \frac{1}{\tan\theta}$$

The calculated values of the strain found to decrease from 5.993x10^{-3} to 3.305x10^{-3} with increasing the power on Mg target. The number of dislocations S_d can be calculated from the following equation:

$$S_d = 1/D$$

It is obvious from table 1 that the number of dislocations decreases with increasing the power on Mg target.

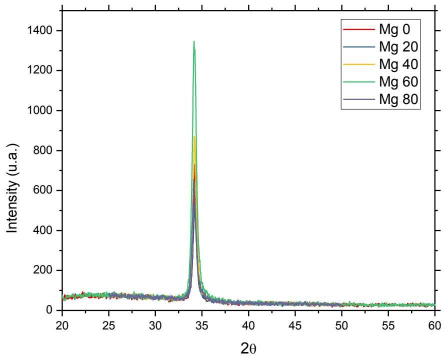

Fig.3: XRD of the Mg-ZnO thin films deposited at different power on Mg target

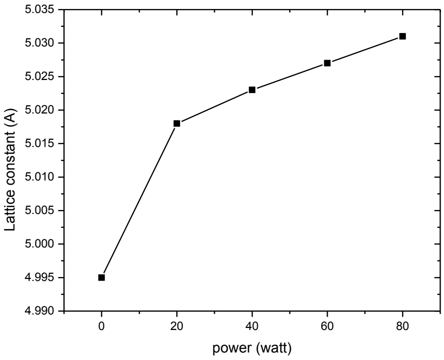

Fig. 4. Variations of the lattice constant with power on Mg target

Table 1. Structural parameters of Mg-ZnO thin films deposited under different power on Mg target

Power on Mg target	2θ	FWHM (°)	Lattice constants(A)	Crystallite size (nm)	S_d x10^7	Interplanar spacing (nm)	Strain x10^{-3}
0.0	34.58	0.28	2.981	26.73	3.741	0.574	3.946
20	34.27	0.85	3,005	9.13	10.953	0.579	5.993
40	34.22	0.60	5.802	13.74	7.278	0.580	5.747
60	34.19	0.48	5.806	17.18	5.821	0.581	3.383
80	34.16	0.50	5.812	16.59	6.028	0.581	3.305

It can be observed from table 1 that as the power on Mg target (reflect the content of Mg) increase starting from 20 watt, the FWHM and strain decrease while the crystallite size, lattice constant and interplanar spacing increase. It can be concluded from table 1 that increasing the power on Mg target improved the crystalline quality of ZnO film effectively.

3.4 Optical properties of the thin films

The optical transmittance spectra of MgZnO thin films deposited under different power on Mg target are shown in Fig. 5. It is clear that the transmittance increases when the power on Mg target and then decreases with more increasing of the power on Mag target.

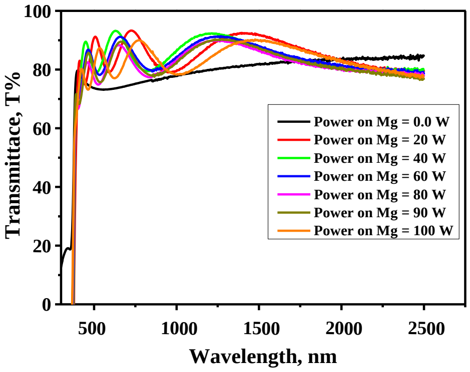

Fig. 5-a. Transmittance spectra of MgZnO films deposited at different power on Mg target

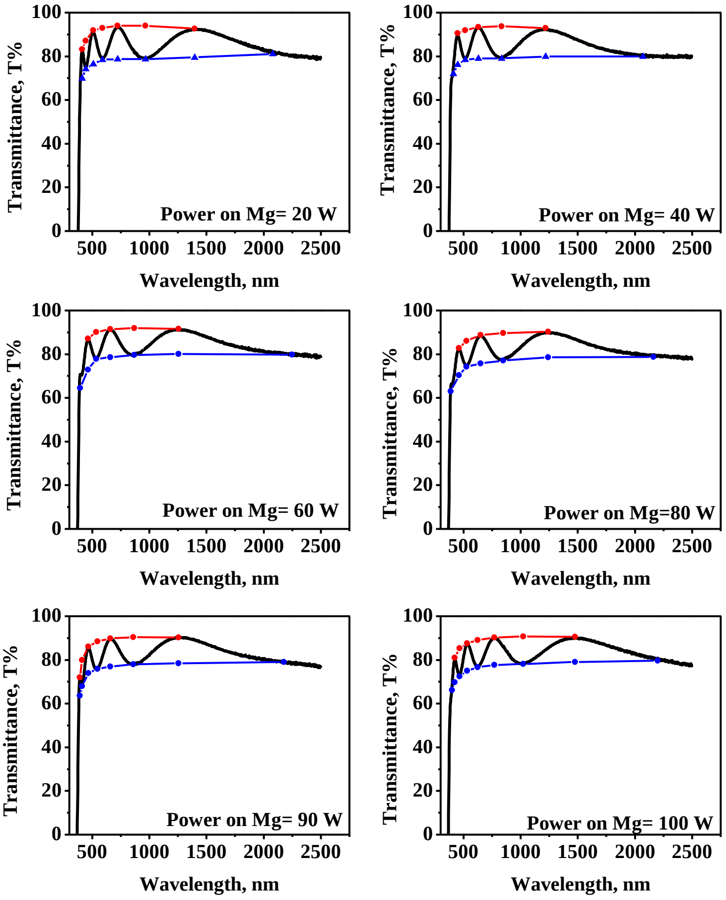

Fig.5-b. Transmittance spectra of MgZnO films deposited at different power on Mg target

The typical UV-VIS-NIR optical reflectance spectra of Mg-ZnO thin films under test are shown in Fig. 6. It is clear that the reflectance decreases with increasing the power on Mg target. This decrease in reflection can be attributed to the surface roughness of the films, which in turn depends on the particle size [32].

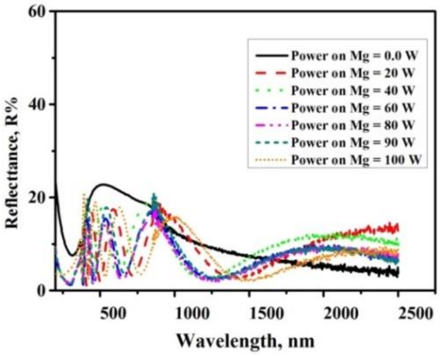

Fig. 6: Reflectance spectra for Mg-ZnO thin films deposited under different power on Mg target

Fig. 7 displays the absorption of the thin films under test, where the absorption decreases in the absorption region which is in consistence to increasing the transmittance in the same region. In addition, the absorption decreases with increasing the power on Mg target.

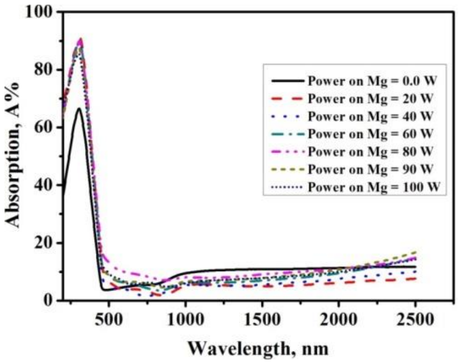

Fig.7. Spectra of the absorption of the films under test

Fig. 8 reveal that the extinction coefficient decreases with increase the power on Mg target which can be owed to the decrease of the absorption coefficient α, where $k = \frac{\alpha\lambda}{4\pi}$.

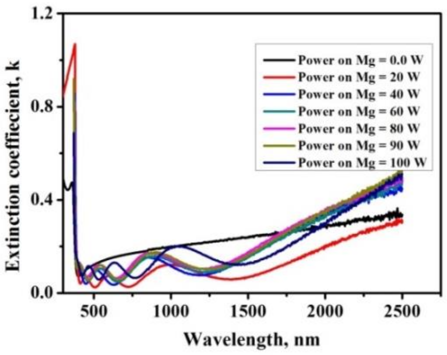

Fig.8: Extinction coefficient spectra for Mg-ZnO thin films deposited under different power on Mg target

Urbach tails were determined using equation 3 from the slopes of the straight lines of the plots as seen in Fig.9-a. The Urbach tails found to decrease in the range of power 0-40 Watt and then increase with more increasing of the power as seen in Fig. 9-b.

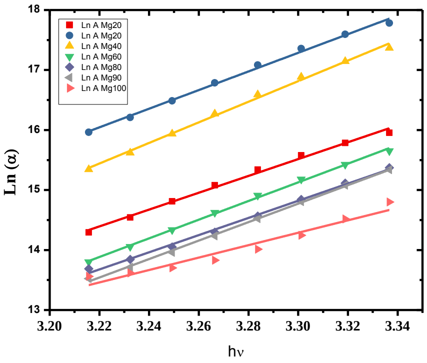

Fig. 9-a: Plots of Lnα vs photon energy for the thin films under test.

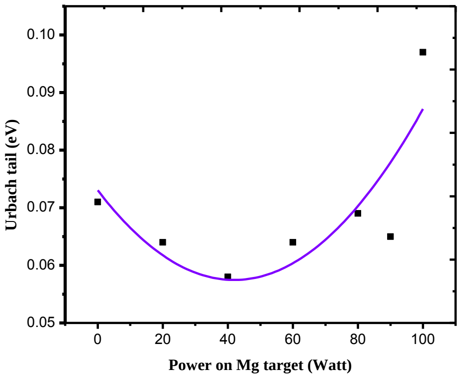

Fig.9-b: Variations of Urbach tail with power on Mg target

The dependence of the optical gap on the power on Mg target is demonstrated in Fig. 10, where it is determined by extrapolating the linear portion of the plots of (αhυ)^2 versus hυ. It is obvious that the optical gap decreases with increasing the power on Mg target. The decrease of the optical gap is attributed to the increase of the particle size [33].

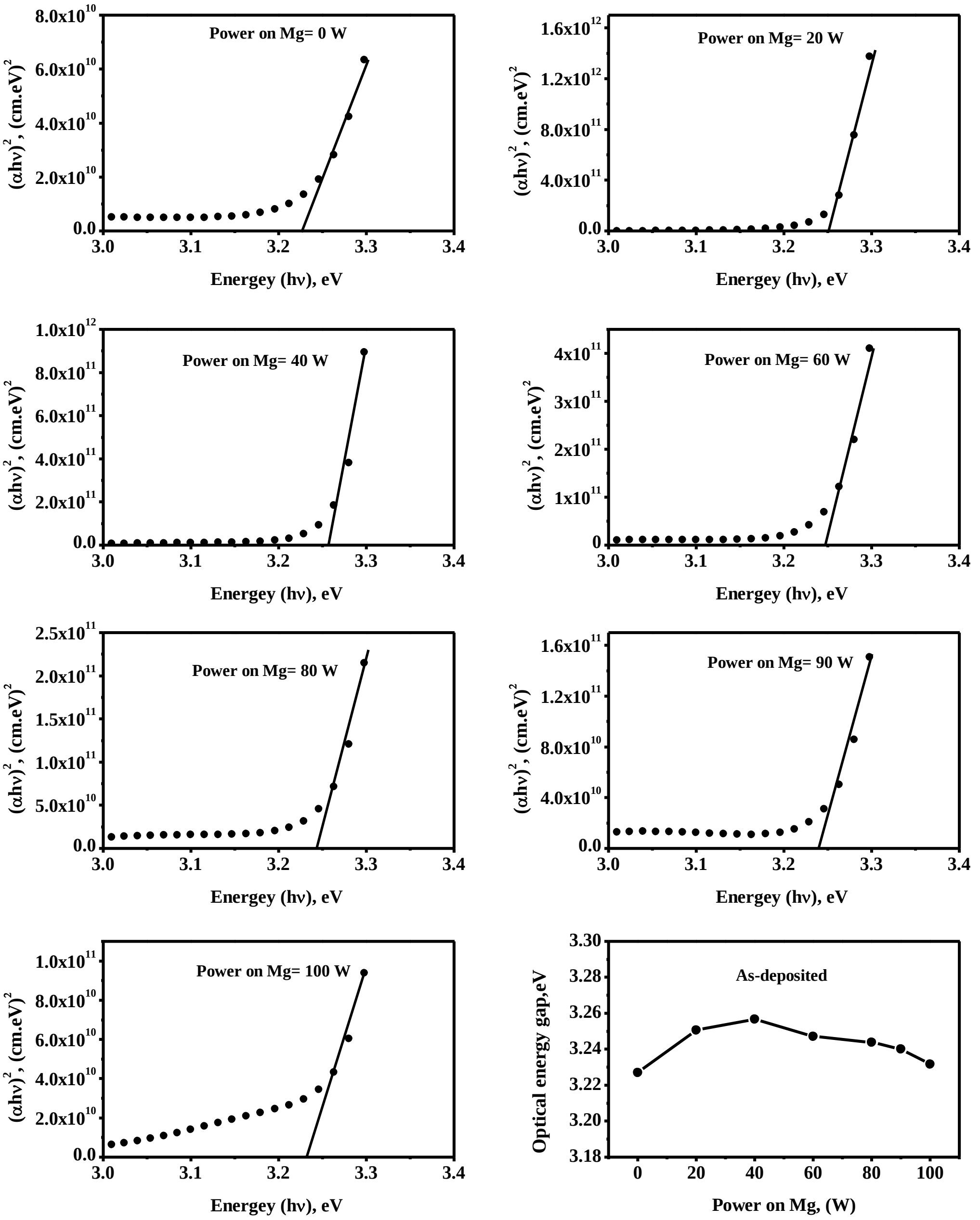

Fig.10: Plot of (αhυ)^2 versus photon energy for Mg- ZnO thin film deposited at different power on Mg target, and the variations of the optical gap with power on Mg target.

The refractive index n found to have the normal dispersion for all films under test as seen in Fig. 11-a. Further, the refractive index decreases in the range of power from 20 watt to 60 watt and then increases with more increasing of the power on Mg target as seen in Fig. 12-b. In addition, the packing density behaves as the refractive index with Mg content.

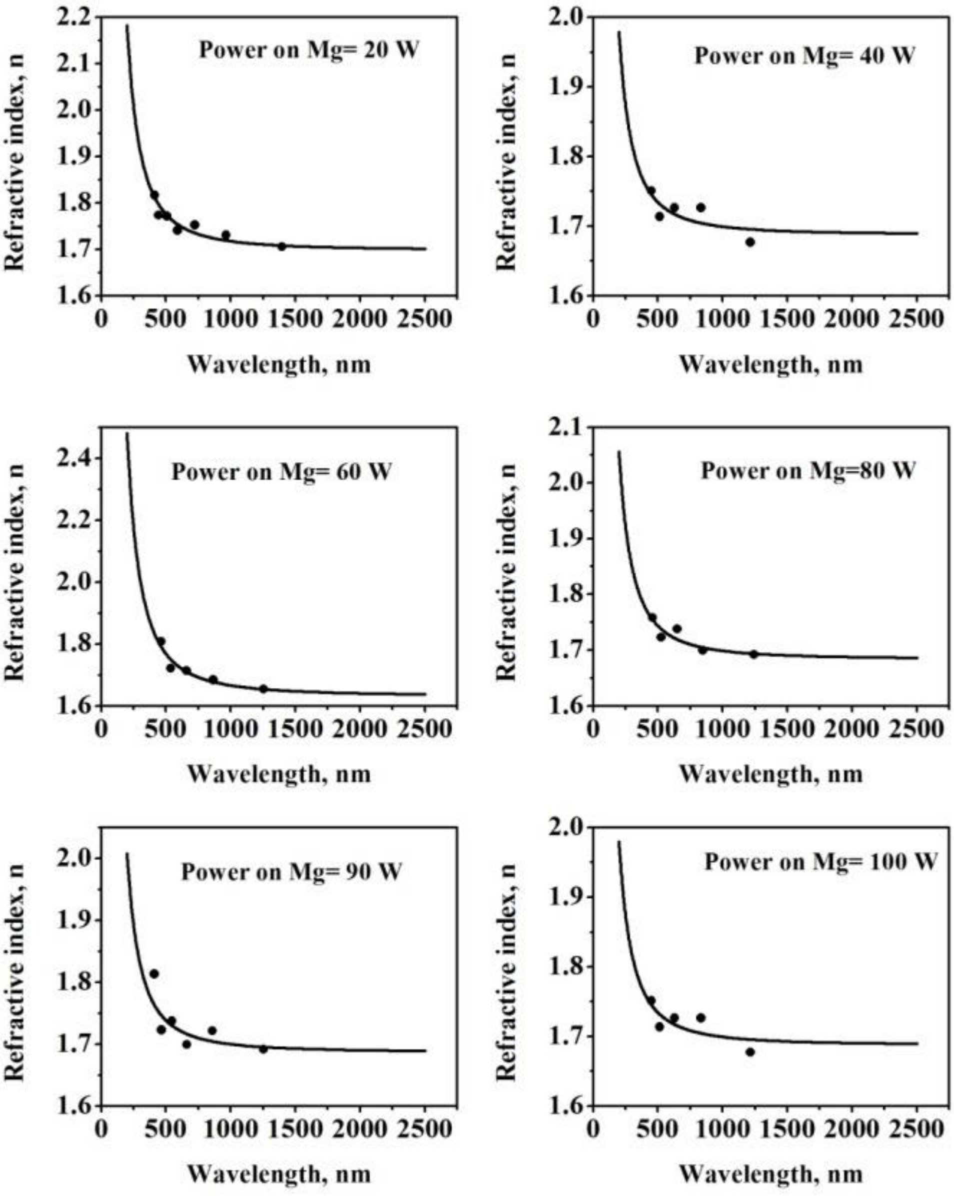

Fig.11-a: Spectra of the refractive index of the films under test.

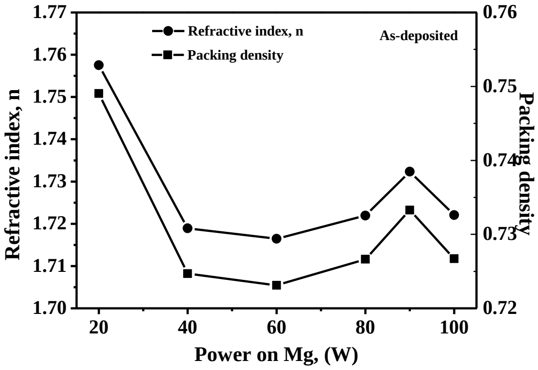

Fig.11-b: Variations of refractive index and packing density with Mg content.

The dielectric constant for the thin films under test found to increase as the Power on Mg increase from 0 to 40 Watt and then decreases with more increasing of the power as seen in Fig.12.

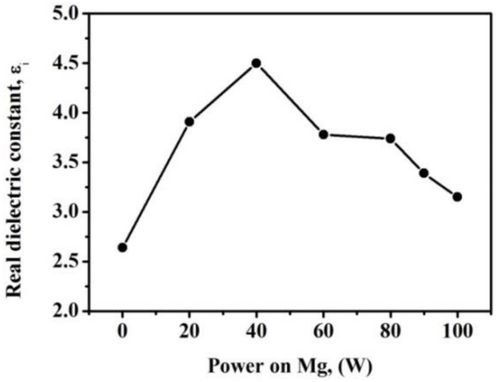

Fig.12: Variations of dielectric constant with power on Mg.

Using eq. 5, the carrier concentration n can be calculated from the slope of the straight lines of Fig. 13-a. The carrier concentration found to increase with increasing the power on Mg target starting from power 20 Watt as seen in Fig. 13-b.

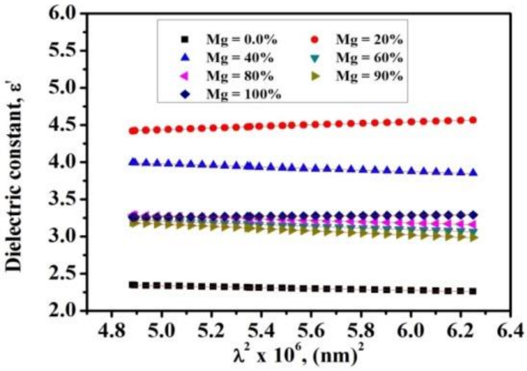

Fig. 13-a: Plots of dielectric constant versus λ^2 for as-deposited Mg-ZnO thin films under different power on Mg target

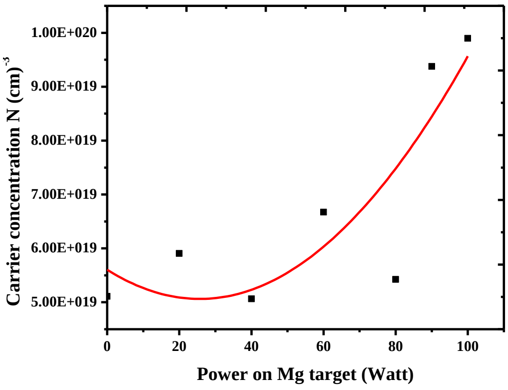

Fig. 13-b: Variations of the carrier concentration with power on Mg target

4. Conclusion

Co-magnetron sputtering was used to prepare Mg-ZnO thin films under powers on Mg target. The X-ray diffraction patterns show crystalline feature. Lattice constant and grain size increase with increasing power on Mg target staring from 20 Watt, whereas, strain and number of dislocation decrease. Urbach tail increases with power on Mg target starting from 40 Watt, whereas, optical energy gap decreases as well as the real dielectric constant. Refractive index behaves as normal dispersion. Carrier concentration increases with increasing the power on Mg target (ratio of Mg).

References

[1] C. F. Yu, S. H. Chen, S. J. Sun, H. Chou, Appl. Surf. Sci. **257,** 6498 (2011).

[2] X. L. Chen, X. H. Geng, J. M. Xue, L. N. Li, J. Cryst. Growth **299**, 77 (2007).

[3] D.J. Cohen, K. C. Ruthe, S. A. Barnett, J. Appl. Phys. **96**, 459 (2004).

[4] R. Hunger, K. Iwata, P. Fons, A. Yamada, K. Matsubara, S. Niki, MRS Proceedings **668**(H2), 8 (2001).

[5] T. Makino, Y. Segawa, M. Kawasaki, A. Ohtomo, R. Shiroki, K. Tamura, Applied Physics Letters **78**(1237), 1 (2001).

[6] Y. Yang, S.S. Hullavard, B. Nagaraj, I. Takeuchi, R.P. Sharma, T. Venkatesan, Applied Physics Letters **82**(3424), 1 (2003).

[7] T. Minemoto, T. Negami, S. Nishiwaki, H. Takakura, Y. Hamakawa, Thin Solid Films **372**, 173 (2000).

[8] I. Hayashi, M.B. Panish, P.W. Foy, S. Sumski, Appl. Phys. Lett. **17**, 109 (1970).

[9] W.I. Park, Y. Gyu-Chul, H.M. Jang, Appl. Phys. Lett. **79,** 2022 (2001).

[10] M.S. Xue, Q.L. Guo, K.H. Wu, J.D. Guo, J. Chem. Phys. **129**, 234707 (2008).

[11] A. Ohtomo, M. Kawasaki, I. Ohkubo, H. Koinuma, T. Yasuda, Y. Segawa, superlattices, Appl. Phys. Lett. **75**, 980 (1999).

[12] W.L. Guana, J. Lianb, Y.X. Yua, Z.Z. Sunb, M.L. Zhao b, X. Wang b, W.F. Zhang, Optik **125**, 5167 (2014).

[13] Joydip Sengupta , Arifeen Ahmed, Rini Labar, Materials Letters **109**, 265 (2013).

[14] A Singh, D Kumar, PK Khanna, A Kumar, M Kumar, M. Kumar, Thin Solid Films **519,** 5826 (2011).

[15] P Sagar, PK Shishodia, RM Mehra, H Okada, A Wakahara, A. Yoshida, Journal of Luminescence **126**, 800 (2007).

[16] Z Ji, Y Song, Y Xiang, K Liu, C Wang, Z. Ye, Journal of Crystal Growth **265**, 537 (2004).

[17] Y Caglar, S Ilican, M Caglar, F Yakuphanoglu, J Wu, K Gao, Journal of Alloys and Compounds **481**, 885 (2009).

[18] Nidhi Adhlakha, K.L. Yadav, Amit Kumar, Piyush Kumar Patel, Jyoti Rani, Meera Rawat, Phys. B Condens. Matter **407,** 3427 (2012).

[19] F.K. Shan, G.X. Liu, W.J. Lee, B.C. Shin, J. Cryst. Growth **291**, 328 (2006).

[20] A. AShrafi, Y. Segawa, J. Appl. Phys. **104**, 123528 (2008).

[21] A. Ghosh, N. Kumari, S. Tewari, A. Bhattacharjee, Indian J. Phys. **87**(11), 1099 (2013).

[22] Xia Zhang, Xiao Min Li, Tong Lai Chen, Ji Ming Bian, Can Yun Zhang, Thin Solid Films **492**, 248 (2005).

[23] Zhao-Hui Li, Eou-Sik Choa, Sang Jik Kwona, Applied Surface Science **314**, 97 (2014).

[24] B.D. Cullity, S.R. Stock, Elements of X-Ray Diffractions, Prentice Hall, Upper Saddle River, NJ, 2001.

[25] H. M. Ali, Phys. Status Solidi A **202**, 2742 (2005)

[26] J. Tauc, Amorphous, Liquid Semiconductors, Plenum Press, NewYork, 1974

[27] Hideyuki Kanazawa, Sadao Adachi, J. Appl. Phys. **83**, 5997 (1998).

[28] E.R. Shaaban, I.S. Yahia, and E.G. El-Metwally, Acta Physica Polonica A, **121,** 628 (2012).

[29] T. S. Moss, G. J. Burrell, B. Ellis, Semiconductor Optoelectronics (Butterworths, London

(1973), p. 71
[30] A. L. Ginting, C. C. Yap, M. Yahya, M. M. Salleh, J. Alloys Compounds. **585**, 696 (2014)
[31] C. Periasamy, P. Chakrabarti, J. Electr. 40 (2011).
[32] P. K. Biswas, A. De, N. C. Pramanik, P. K. Chakraborty, K. Ortnerb, V. Hockb, S. Koder, Materials Letters **57**, 2326 (2003).
[33] M. Bellardita, M. Addamo, A. Di Paola, L. Palmisano, Chemical Physics **339**, 94 (2007).